# High Power Microwave Plasma Beam as A Heat Source (Report I)†

# —Microwave Plasmotron in Nitrogen Gas—

**Yoshiaki ARATA*, Shoji MIYAKE** and Sadao TAKEUCHI*****

**Abstract**

*A 3 kW-class microwave plasmotron in nitrogen is investigated. The dimension of the plasma flame becomes 10 cm in length and 0.5 cm in diameter in a typical operation. The plasma attains a temperature about 6700°K and its density 7 $\times 10^{13}$ $cm^{-3}$ near the hottest part of the plasma. A remarkable spatial nonuniformity of the plasma conductivity is observed. A large gas flow rate ($30 \leq \phi \leq 200$ l/min) strongly affects the dimension and the energy transfer process of the plasma. The measurement of the plasma impedance gives a qualitative agreement with the rod model of the plasma. Some theoretical discussions are performed on the energy balance problems and compared with the experimental results.*

## 1. Introduction

Several types of plasmas in a steady state operation at atmospheric pressure were employed for various engineering purposes, using "plasmotron" such as plasma jet or induction torch, etc. As for the plasma jet, many kinds of torches have been produced and developed and they are utilized in practice up to the power level of 1 MW for welding, cutting, melting, chemical reactions and so on. Their physical processes have also been intensively studied by many researchers. RF plasmotron[1)~2)] (named after induction torch) which has a frequency range from 1 MHz to 30 MHz is applied for chemical reaction processes or spectroscopic sources etc., with a power level of several tens of kilowatts.

Microwave plasmotrons with f=1~10 GHz were also developed on a coaxial waveguide[3)~5)] or on a rectangular one.[6)] But the power level employed in such cases was about 1 kW at most and it was not used as a practical processing heat source. Recently "optical plasmotron" prepared by $CO_2$ Laser energy was proposed by Yu. P. Raizer[7)~8)], and its power was only about 200 watts. But we predict that its fundamental properties will be studied as a practical heat source.

The physica character of the plasma jet obtained with these DC plasmotrons is generally believed to be in a thermal equilibrium state with the temperature below several eV. Plasmas in RF plasmotrons are also said to be in LTE (local thermal equilibrium state)[1)], but its deviation for the typical plasma parameters has been reported by several researchers.[9)~10)] As for microwave plasmotron some authors[5)~6)] report that the plasma is in LTE but others report[3)~4)] that it is not in LTE. This is because the plasma processes strongly depend on gas type, gas flow rates, incident microwave energy and so on, and no systematic investigation have been performed until now.

Recently, P. L. Kapitza and his group[11)] have studied plasmas in several types of cavity resonators above atmospheric pressure and they succeeded in producing a fully ionized plasma with electron temperature $T_e \simeq 100$ eV, by using a cylindrical cavity resonator where deutrium or helium gas is circulated in a vortex form at the pressure 1~3 atm. Using CW microwave energy of 175 kW with f=1.55GHz, the maximum power absorbed to the plasma was about 20 kW. The plasma dimension reached to 10 cm in length which is nearly equal to half a wavelengh and about 1 cm in diameter. Its state was in a high degree of nonequilibrium between the electrons and the heavy particles. It is recognized that this method is quite unique and introduces some new atmospheric plasma processes which have never been obtained to date. A mechanism was proposed to sustain ultra-high temperature "plasma lump", which was enclosed with such a plasma boundary as the electric double layer and separated from cold high pressure gas. It still remains left behind to clarify several problems, theoretically and experimentally Nevertheless, this plasma process encourages us to study the high power microwave atmospheric plasma beam as a new type

† Received on Nov. 25, 1972
* Professor
** Research Instructor
*** Graduate Student

of practical heat source.

Using a 3 kW-class (f=2.45 GHz) microwave plasma torch similar to the one employed in ref. 12), some systematic studies on "microwave plasmotron" are reported in this paper, with data on different types of gas, gas flow rates and incident microwave powers. Spectroscopic and electric diagnostic techniques were employed to determine plasma dimension, its conductivity, temperature, and their spatial distributions, etc. These results were compared with some theoretical considerations pertaining electrodynamic and thermodynamic plasma processes ocurring in microwave plasmotron.

## 2. Experimental Procedures

### 2.1 Experimental Apparatus

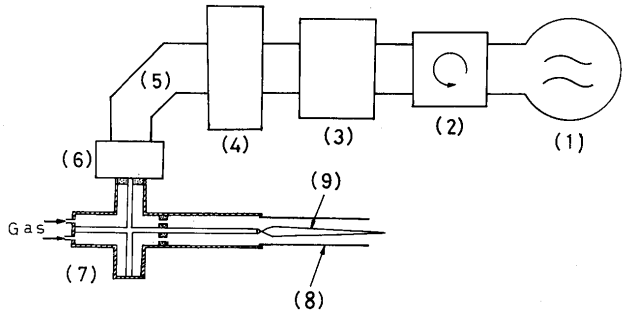


Fig. 1. Schematic diagram of experimental apparatus; (1) magnetron, f=2.45 GHz, $P_{max}$=3 kW, CW., (2) circulator, (3) standing wave meter, (4) directional coupler, (5) E-corner, (6) coaxial transformer, (7) plasmotron forming a coaxial waveguide, (8) quartz pipe with 20 cm in length and 3.7 cm in diameter inserted in the outer conductor, (9) plasma flame.

**Figure 1** shows a schematic diagram of the experimental apparatus. Ultrahigh frequency (UHF) oscillation with a frequency f=2.45 GHz generated by a magnetron (1)* is transmitted in a rectangular waveguide with $TE_{01}$ mode through circulator (2), standing wave meter (3), and directional coupler (4); to a coaxial transformer (6), where TEM type oscillation is produced and it enters into the plasmotron (7) having a coaxial waveguide (17 mm o. d. × 39 mm i. d. ) with two tuning plungers. UHF power from the magnetron can be varied continuously up to 3 kW. Discharge gases are axially introduced into the coaxial wave guide through a gas inlet at the bottom end in the range of flow rates from 30 to 200 *l*/min.

The discharge is ignited at the open end of the plasmotron where a water cooled tungsten electrode is placed on the tip of the inner conductor. A quartz pipe (8), 20 cm in length, is set to obtain a stable axial flow of the gases. In this study, nitrogen and a mixture of 5 % hydrogen into nitrogen were mainly used as a plasma forming gas, although various gases as indicated in **Table 1** were also tried.

* ( ) refer to Fig. 1.

Table 1. Operating Condition.

| | |
|---|---|
| Micro-wave frequency | f = 2.45 GHz |
| Micro-wave power of magnetron | $P_i$ = 0.2~3kW |
| Plasma-forming gases | $N_2$ & $N_2$+5%$H_2$(mainly), Air, $CO_2$, Ar, Ar+2~10%$H_2$ |
| Flow rate of gas | Φ = 30~200 l/min |

The circulator (2) with a matched load serves to protect the magnetron from the incidence of a large reflected power. With a universal power meter connected to the directional coupler (4), the reflected power is detected and the standing wave meter (3) is used to determine plasma impedance for various plasma parameters.

### 2.2 Measurement of Microwave Radiation

Microwave radiation from the open end of the plasmotron into space is measured, using a loop antenna with 2 mm in the loop radius and 0.5 mm in the lead radius, and the loop efficiency is estimated at about 8 %.[13] Spatial distributions of the radiation were detected, by revolving the loop axially or radially with a motor-driven unit. In **Fig. 2** is shown a block diagram of the radiation detection system.

To obtain some relations between wave propagation and plasma formation, a CdS cell is set at the same position with the antenna as also indicated in **Fig. 2.**

### 2.3 Spectroscopic Measurements

The principal problem in the study of the plasma itself is the determination of the electron density $N_e$, the ion density $N_i$, the neutral particle density $N_o$ and also their temperatures $T_e$, $T_i$ and $T_o$. Determination

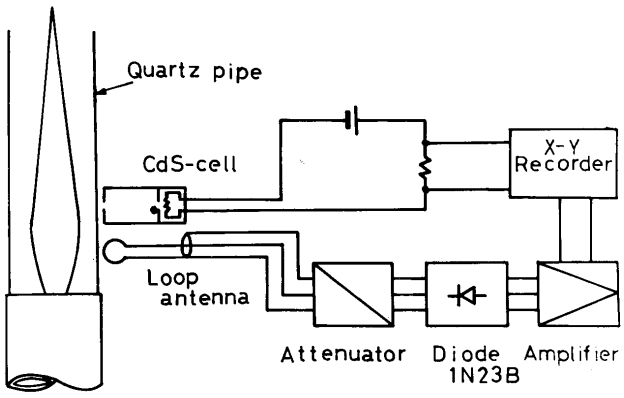


Fig. 2. Block diagram of microwave radiation and light emission measurement system. The radiation is detected with a loop antenna and the total light emission from the plasma flame with a CdS cell.

of the electron density can be acomplished frequently, using the Stark effect in the visible part of the spectrum by measuring the broadening of a spectral line. For this purpose, the hydrogen Balmer line $H_\beta$ was obtained by mixing 5 % $H_2$ into $N_2$ gas. From the broadening $\Delta\lambda$, its Stack effect part $\Delta\lambda_S$ was determined, and we have[14]

$$N_e = C(N_e, T)\Delta\lambda_S^{3/2} \quad (1)$$

where C is the numerical factor that has a very weak dependence on temperature and it is tabulated in ref. 14) with $\Delta\lambda_S$ in Å.

As for the temperature determination we assume hereafter that the plasma is in LTE. Then from the Saha- Eggert equation,[15]

$$\frac{N_{r+1}N_e}{N_r} = \frac{2U_{r+1}(T)}{U_r(T)} S_r^*(T), \quad (2)$$

$$S_r^*(T) = 2.4125\times10^{15} T_e^{3/2} e^{-\frac{E_r - \Delta E_r}{kT}} \ [cm^{-3}], \quad (3)$$

where $N_r$, $N_{r+1}$=number density of all r— and (r+1)—fold ionized atoms [$cm^{-3}$]; $U_r$, $U_{r+1}$=partition function of r—and (r+1)—fold ionized atoms; k=Boltzman's constant; $E_r$=ionization energy for ionization r→(r+1); $\Delta E_r$=lowering of ionization energy; $T=T_e=T_i=T_o$ [°K], we can obtain the plasma temperature T combining the data listed in ref. 15) and the measured electron density. Moreover it is considered in this case that the nitrogen temperature is equal to that of hydrogen. The assumption of LTE is admissible at least for nitrogen or air at atmospheric pressure as is generally stated in the results of arc plasma.

In order to obtain exact line widths we have employed a monochrometer (GE—100, 1 m Ebert type) with the first order dispersion 8.3 Å/mm. The resolving power of the monochrometer was calibrated by measuring the emission spectrum of a low pressure mercury discharge tube and the instrumental half-width is 0.15 Å with the exit slit width of 15 $\mu$. The width of the entrance slit is fixed at 30 $\mu$.

The optical system is shown in **Fig. 3.** The measurement is made perpendicular to the plasma flame. To measure the emission from the limited zone of the plasma and to shield the microwave radiation, a copper cylinder (3)** movable in the axial direction is set over the quartz pipe (2), and it has a slit (4) of 4.5 mm in width cut over a semicircumference. The change in the reflected power due to the setting of this cylinder was very small, so that the effect of the cylinder to the plasma character was negligible. The emission from this limited plasma is focused on a slit S(6) (0.8 mm in width) set in front of a crystal lens $L_2$

** ( ) refer to Fig. 3.

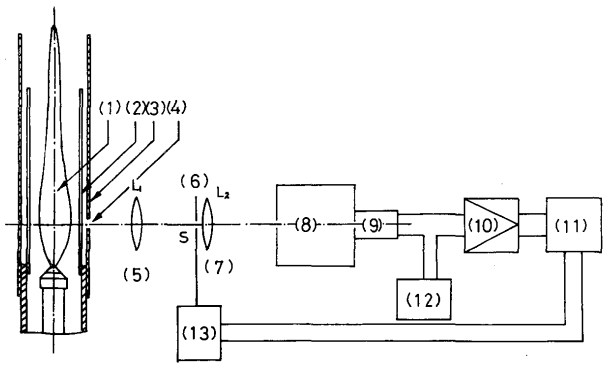


Fig. 3. Schematic diagram of optical system; (1) plasma flame, (2) quartz pipe, (3) copper cylinder with a slit (4) of 4.5 mm in width cut over a semeicircumference, (5) and (7) crystal lenses $L_1$ and $L_2$ respectively whose aperture is 1.7 cm and the focal length 8 cm, (6) movable transverse slit S of 0.8 mm in width, (8) monchrometer (GE—100, Ebert type, lst order dispersion 8.3 Å/mm), (9) photomultiplier tube (R212 UH), (10) DC amplifier, (11) X-Y recorder, (12) DC high voltage source, (13) motor-driven system.

(7). Axial intensity distribution is measured by moving the copper cylinder and the monochrometer at the same rate, and the radial distribution is obtained by scanning the slit (6) transversely. Thus the spatial scanning of the monochromatic emission are detected by a photomultiplier (9) and recorded on an X-Y recorder (11).

## 3. Experimental Results

### 3.1 Profile of Plasma Flame for Different Gases

Typical photographs of the plasma flame are shown in **Figs. 4～9** for nitrogen, air, carbon dioxide, helium, argon and mixtures of argon and hydrogen respectively. The discharges with molecular gases **(Figs. 4～6)** show stable characters even for high powers and the reflected power is small. The plasmas in rare gases **(Figs. 7～8)** have large power reflection and are less stable. Moreover, the flash over between the inner and the outer conductors tends to occur more frequently in these gases. It is farily difficult to raise the incident power more than 1 kW. The situation changes abruptly, however, when we admit several percentages of hydrogen (2～10 %) into these gases. In general, the more the percentage of hydrogen, the more the stability increases and the reflected power decreases. Moreover, the hydrogen-mixed discharge provides a filamentary-like core as shown in **Fig. 9** or as stated in ref. 11).

As for the flash over of the discharge, it means that a plasma tends to occur along the electric lines of force, which is directed radially in the coaxial waveguide. Then to avoid the flash over it is better to have a discharge directed parallel to the electric field (for instance as indicated in ref. 6) ).

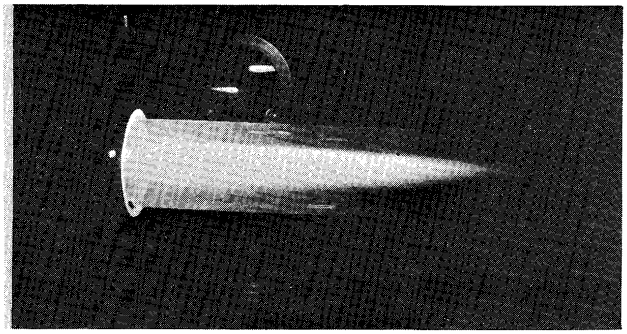

Fig. 4. Photograph of $N_2$ plasma; $P_t$=1.9 kW, $\phi$=51 *l*/min.

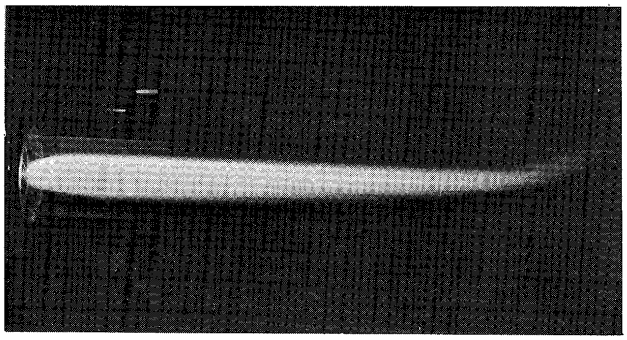

Fig. 5. Photograph of air plasma; $P_t$=1.9 kW, $\phi$=52 *l*/min.

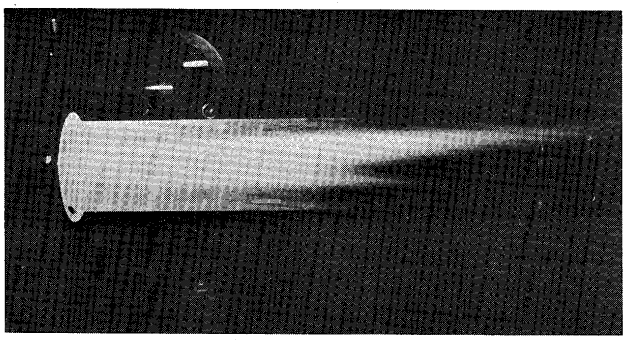

Fig. 6. Photograph of $CO_2$ plasma; $P_t$=1.44 kW, $\phi$=40 *l*/min.

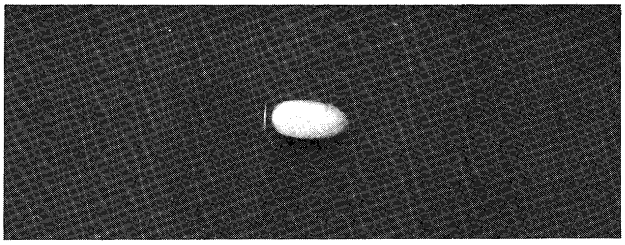

Fig. 7. Photograph of He plasma; $P_t$=0.8 kW, $\phi$=133 *l*/min.

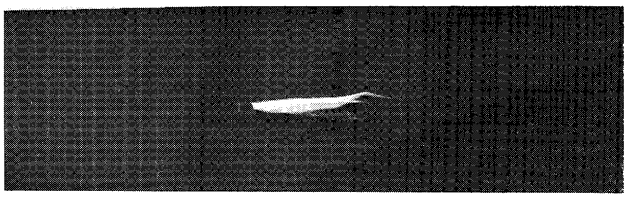

Fig. 8. Photograph of Ar plasma; $P_t$=0.4 kW, $\phi$=42 *l*/min.

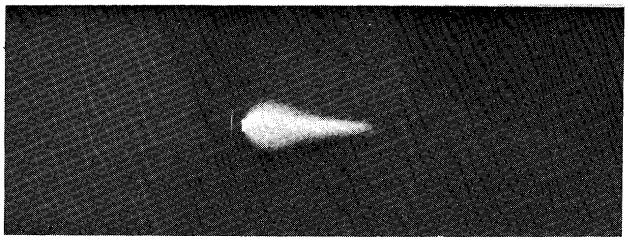

Fig. 9. Photograph of Ar+10 % $H_2$ plasma; $P_t$=0.78 kW, $\phi$=43 *l*/min.

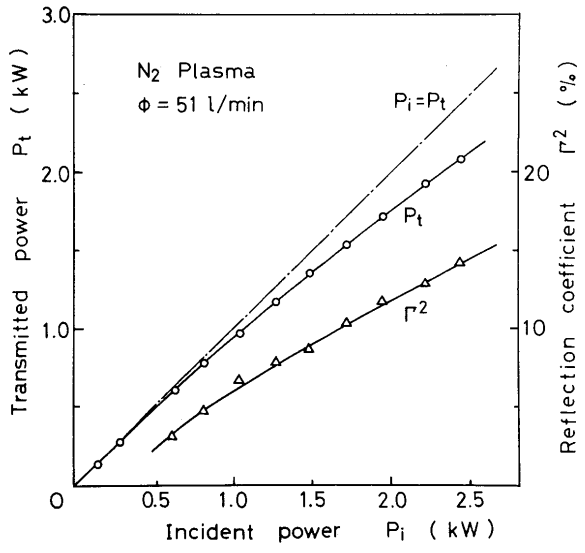


Fig. 10 Plots of transmitted power $P_t$ and reflection coefficient $\Gamma^2$ for various incident powers $P_i$; $P_t=P_i(1-\Gamma^2)$.

### 3.2 Wave Propagation and Power Absorption

In **Fig. 10** the transmitted power, $P_t$ from the open end of the plasmotron into the plasma beam and the space is plotted for various incident powers, $P_i$ to the plasmotron. The line of $P_i=P_t$ means the case where there is no reflection of power. It is clear that the plasma acts as a well matched load to the wave and the reflection coefficient is about 15 % at the power level of 2.5 kW, which increases nearly proportionally to the incident power.

The radial distribution of the wave transmitted into space from the plasmotron without plasma is shown in **Fig. 11 (a).** The radiation intensity at z=1 cm is almost constant at $0 \leq r \leq 8$ mm. This distribution clearly corresponds to that of the wave in the coaxial waveguide. Its intensity is proportional to the transmitted power as shown in **Fig. 11 (b),** which confirms the good response of the loop antenna. The

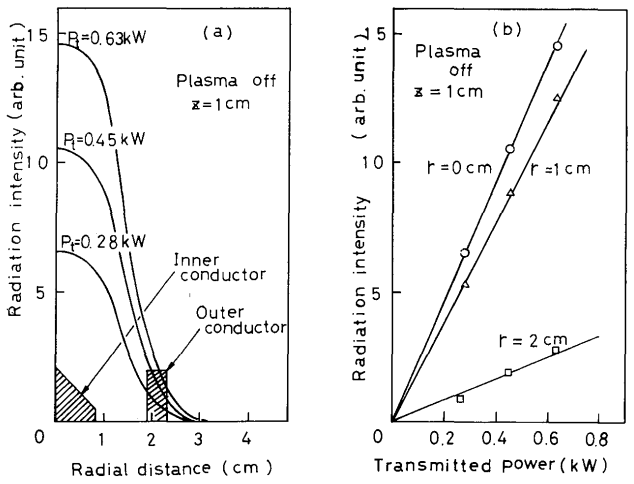


Fig. 11. (a) Radial distribution of microwave radiation in the absence of plasma. The measurement is performed at z=1 cm.
(b) Radiation intensity versus transmitted power at different radii.

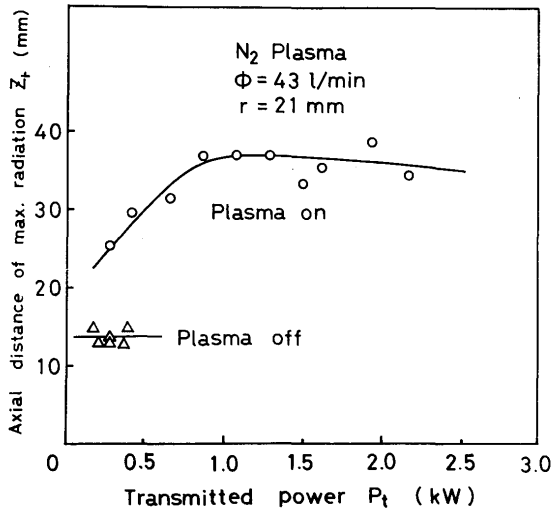


Fig. 13. Plots of the axial distance $z_r$ where the maximum microwave radiation at r=21 mm is observed for various transmitted powers.

axial radiation distribution shows the maximum value at the open end (z=0 cm) with the optimum matching, which is generally expected in the microwave theory.

In general it is so difficult to obtain a real distribution of the wave in the core of the plasma beam that it is measured at the surface of the quartz pipe as sketched in **Fig.14. Figure 12** shows the axial distribution of the radiation measured at r=21 mm and the light emission from the plasma measured with a CdS cell. The distance that gives the maximum radiation intensity shifts due to the plasma formation. The relation between the axial distance which gives the maximum radiation $z_r$ and the transmitted power is given in **Fig. 13.**

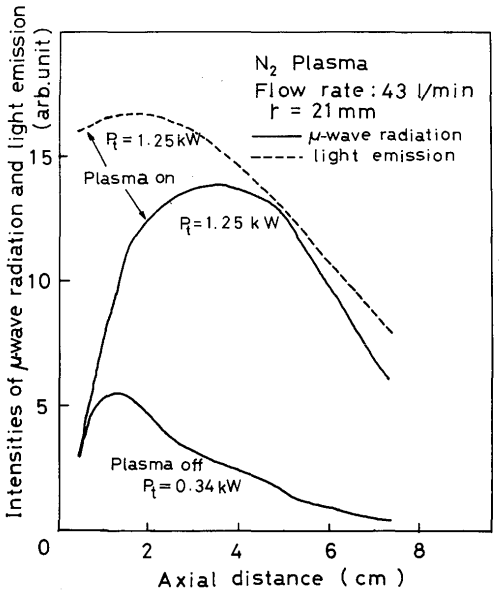


Fig. 12. Intensity distribution of microwave radiation into space and light emission from a plasma in the axial direction at r= 21 mm.

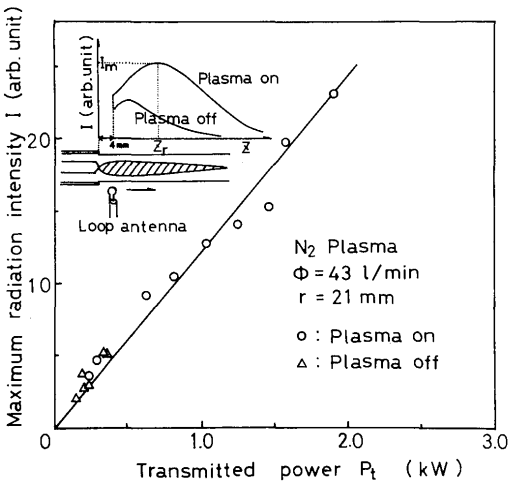


Fig. 14. Relation between maximum intensity of microwave radiation at $z_r$ and transmitted power $P_t$.

In case of no plasma, $z_r$ does not change, but when the plasma is firing it increases up to 35 mm with $P_t$ and after that it shows nearly constant value at $P_t \geq$ 0.8 kW. Meanwhile **Fig. 14** shows a dependence of the maximum intensity on the transmitted power. In both cases, with or without plasma, it is proportional to the transmitted power and lies on the same line. This means that the microwave energy in this region (r=21 mm) has no effect on the power absorption to the plasma. The plasma absorbs the wave energy in the region of $0 \leq r \leq 8$ mm, as the plasma radius is below 3 mm for the maximum incident power (see **Fig. 17).**

It is certified with a spectrum analyzer that the output signal of the loop antenna gives only the signal of the wave transmitted from the plasmotron.

### 3.3 Configurations of the Plasma

As stated in Sec. **3.1,** the nitrogen plasma beam is so stable and efficiently absorbs the wave power with a configuration shown in **Fig. 4.** When the CdS cell is moved along this plasma axis at the radial point r=21 mm, the maximum point of light emission is obtained as indicated by the dotted line in **Fig. 12.** Although the dotted line gives total amount of the light emitted from the plasma beam toward the cell the real spatial intensity distribution of the monochromatic light emission is given in **Fig. 18.** The distance of the maximum light emission, $z_l$ changes with the power as shown in **Fig. 15** and it has a similar character as that of the microwave radiation and reaches a value of about 15 mm when $P_t \geq 0.8$ kW.

Length of the plasma flame, L is determined using the axial length of half-height of the emission distribution measured from the end of the plasmotron as sketched in **Fig. 16.** It increases in proportion to $P_t$ and becomes about 10 cm at $P_t=2.0$ kW. The plasma diameter, D is determined using the half width of the radial distribution of the monochromatic radiation ($H_\beta$ line) measured with the movable slit S in **Fig. 3.** A sample record of the radial intensity distribution of $H_\beta$ line is shown in **Fig. 23.** The plasma diameter also increases with the transmitted power as shown in **Fig. 17** and has about 5 mm at $P_t=2.5$ kW. The axial dependence of the plasma beam diameter obtained from the data of **Fig. 18,** is shown in **Fig. 19.**

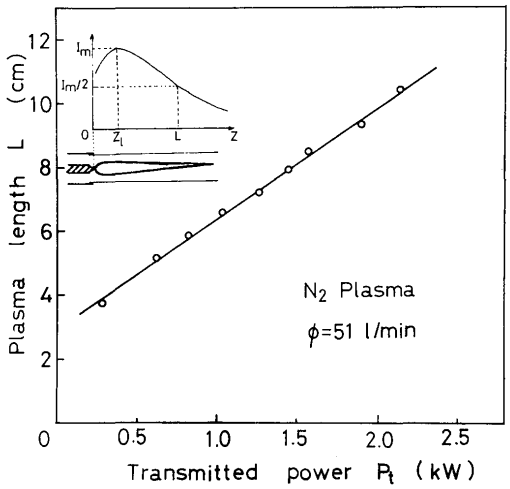


Fig. 16. Dependence of plasma length L on transmitted power $P_t$. L is determined the from half-height of the intensity distribution of light emission as is sktched in the figure.

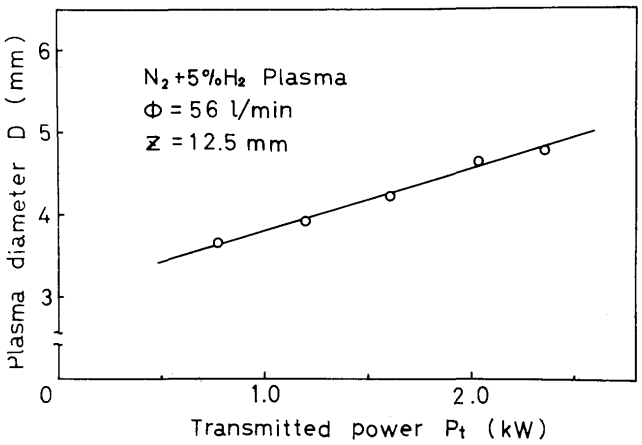


Fig. 17. Relation between plasma diameter D and transmitted power $P_t$. D is determined from the half-width of the radial intensity distribution of $H_\beta$ line.

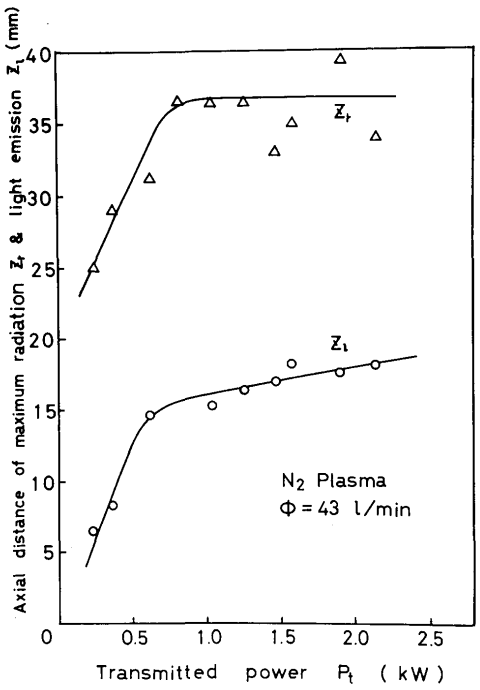


Fig. 15. Plots of axial distance $z_r$ of maximum radiation intensity and that of light emission $z_l$ against transmitted power.

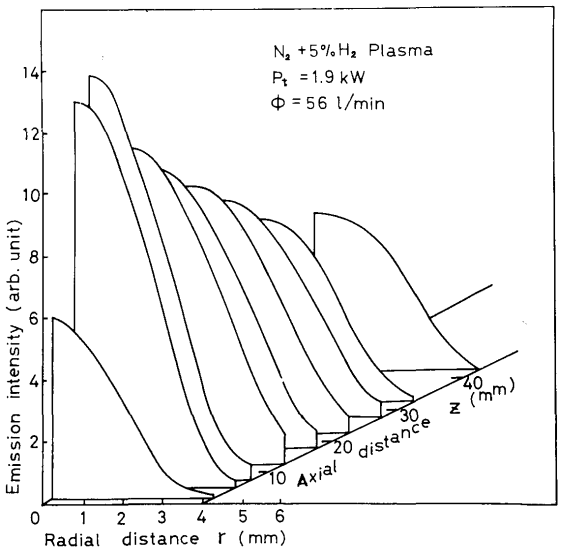


Fig. 18. Spatial intensity distribution of $H_\beta$ line for $P_t=1.9$ kW, $\phi=56$ l/min.

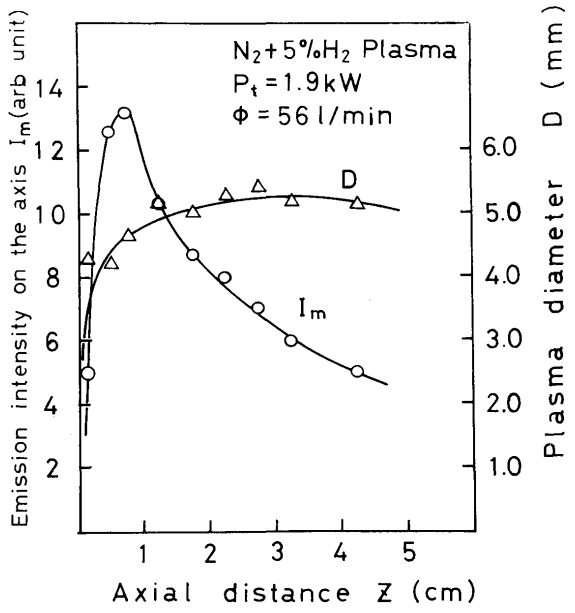


Fig. 19. Axial intensity distribution of $H_\beta$ line and change of plasma diameter D in the axial direction.

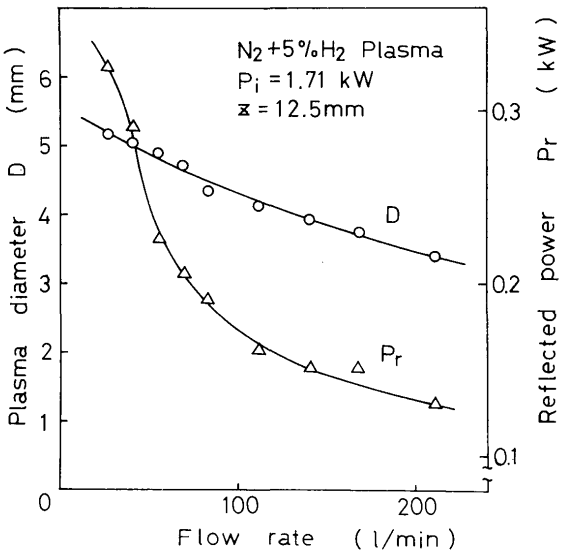


Fig. 20. Change of plasma diameter D and reflected power $P_r$ with gas flow rate.

It becomes about 5 mm at z=15 mm and is nearly constant up to z=4 cm, while the intensity of the $H_\beta$ line on the axis indicates the maximum value at z =0.75 cm and falls rather sharply with the distance. The microwave energy seems to be absorbed to the plasma beam between $0 \leqq z \leqq 15$ mm.

Both the plasma diameter and the reflected power decrease with an increase in the gas flow rate as shown in **Fig. 20.**

### 3.4 Measurement of Plasma Impedance

Employing the standing wave meter (3) indicated in **Fig. 1,** the plasmotron impedance was measured. The reference plane of the impedance measurement in the rectangular waveguide system is set along the center axis of the coaxial transformer (6) and the characteristic impedance of the rectangular waveguide is 462 $\Omega$. The impedance obtained in this manner gives the same character that the plasma torch shows itself.

**Figures 21** and **22** show the effects of the transmitted power and the gas flow rate on the plasma impedance respectively. The resistance of the plasma increases sharply with increasing the power, and it

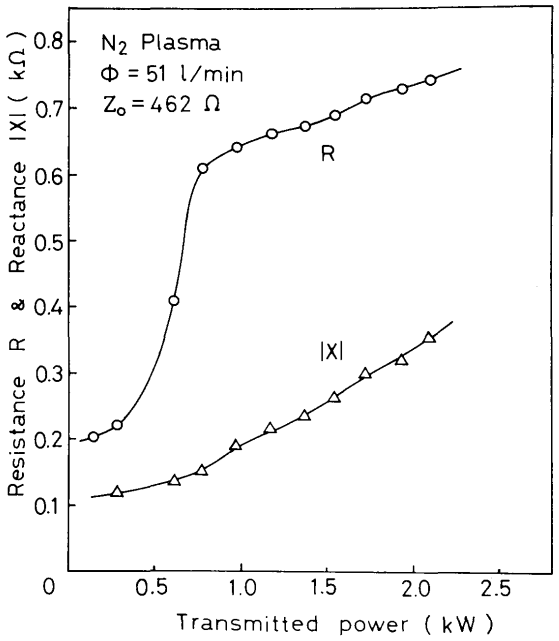


Fig. 21. Plasma impedance for various transmitted powers. R is resistance and X is reactance (actually capacitance). The reference plane is chosen at the coaxial transformer. Characteristic impedance of the rectangular waveguide is 462 $\Omega$.

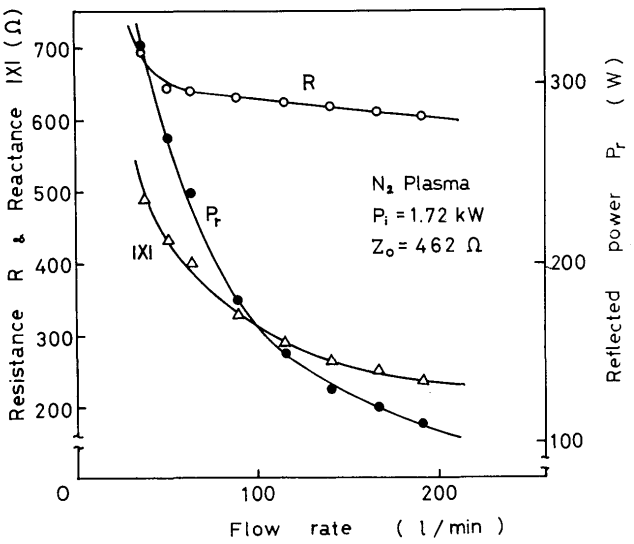


Fig. 22. Dependence of plasma impedance on gas flow rate.

becomes 600 $\Omega$ at $P_t$=0.8 kW and after that, the increases is gradual. It has a similar tendency with the data of **Fig. 15.** Meanwhile the reactance (in fact it is the capacitance) changes almost proportionally to the power input.

### 3.5 Plasma Temperature and Its Density

The electron density of the plasma beam was obtained, measuring the broadening due to the Stark effect, that is, the line width of hydrogen Balmer series, $H_\beta$ line. **Figure 23** shows an example of the spectrum profile and its radial distribution. The plasma temperature is estimated using Saha-Eggert equation with the assumption of local equilibrium state (LTE) of the plasma. The axial distribution of the plasma temperature and its density is plotted in **Fig. 24.** They increase quite abruptly and attaines the maximum value, T=6700°K, $N_e=7\times10^{13}$ cm$^{-3}$, at z= 5 mm and then decrease moderately with the axial distance. The radial distribution of the plasma temperature is shown in **Fig. 25,** though the Abel inversion of the intensity distribution is not performed. It decreases moderately with the radial distance.

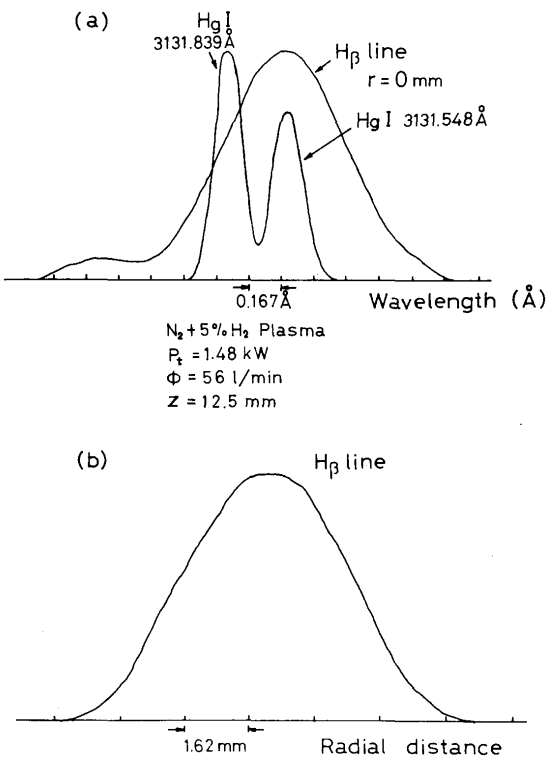


Fig. 23. Sample records of $H_\beta$ line emission. (a) Wavelength scanning of the line, where the spectra of HgI are also traced for comparion. From HgI spectra the instrumental half-width of the monochrometer is decided as 0.15 Å. A small peak in $H_\beta$ spectrum comes from nitrogen spectrum. (b) Radial intensity distribution of $H_\beta$ line.

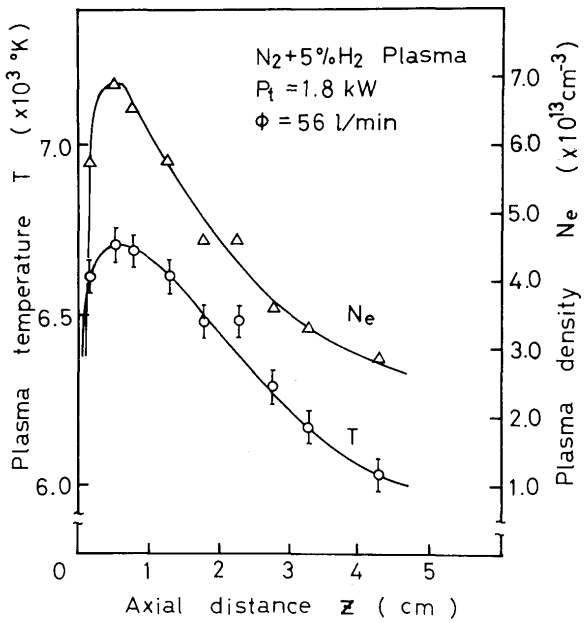


Fig. 24. Axial distribution of plasma temperature and its density for $P_t$=1.8 kW, $\phi$=56 *l*/min. The plasma temperature is estimated from eqs. (2)~(3).

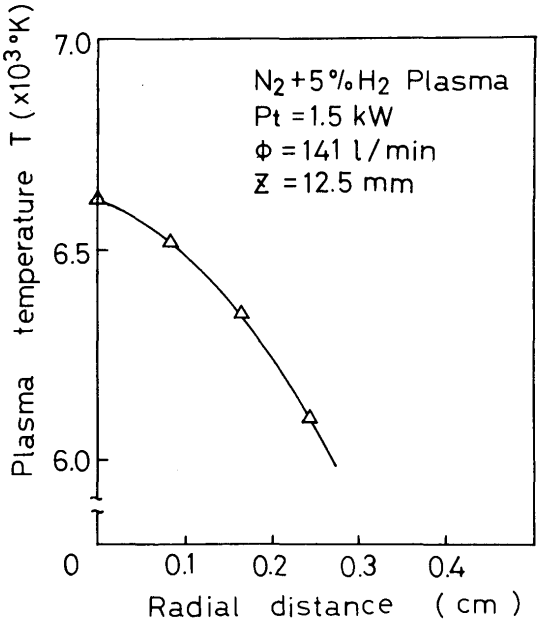


Fig. 25. Radial distribution of plasma temperature for $P_t$=1.5 kW, $\phi$=141 *l*/min.

The effects of both the transmitted power and the gas flow rate on the plasma temperature are shown in **Figs. 26~27.** The plasma temperature increases nearly proportionally to the power when $P_t \geqq 0.8$ kW. The change of the gas flow rate slightly affects the plasma temperature or its density as shown in **Fig. 27;** that is, the temperature keeps about 6600~6650°K at $30 \leq \phi \leq 200$ *l*/min.

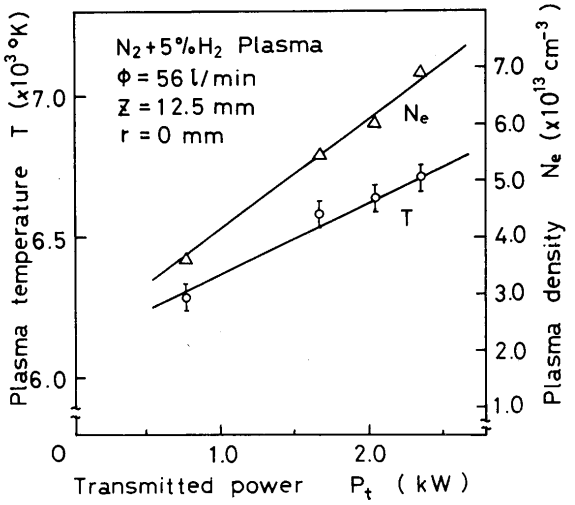


Fig. 26. Dependance of plasma temperature and its density on transmitted power for $\phi$=56 *l*/min. The measurement is performed at z=12.5 mm, r=0 mm.

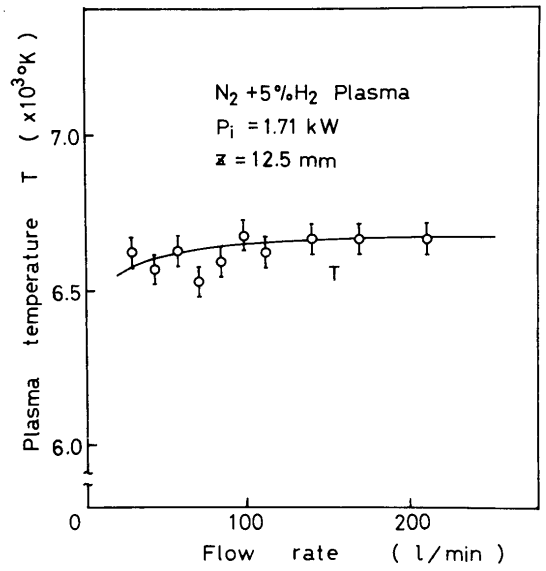


Fig. 27. Dependence of plasma temperature on gas flow rate for $P_t$ =1.71 kW, z=12.5 mm, r=0 mm.

## 4. Theoretical Considerations and Discussions

When a plane electromagnetic wave, $\mathbf{E}=\mathbf{E}_0 e^{i(\omega t-kz)}$ propagates in a uniform plasma, electrical conductivity, $\sigma=\sigma_r-i\sigma_i$ and dielectric constant, $\varepsilon$ of the plasma are defined from elementary theory[16]

$$\sigma_r=\frac{e^2N_e\nu_{eff}}{m(\omega^2+\nu_{eff}^2)}, \quad \sigma_i=\frac{e^2N_e\omega}{m(\omega^2+\nu_{eff}^2)},$$
$$\varepsilon=1-\frac{4\pi e^2N_e}{m(\omega^2+\nu_{eff}^2)}=1-\frac{4\pi\sigma_r}{\nu_{eff}}=1-\frac{4\pi\sigma_i}{\omega}, \quad (4)$$

where $\sigma_r$, $\sigma_i$=real and imaginary part of the conductivity, and m, e=electron mass and charge, respectively, and $\omega$=wave frequency, $N_e$=plasma density, and $\nu_{eff}$=effective collision frequency of an electron. Considering that the direction of the wave propagation is along the axial direction, the wave number k is connected with index of refraction $n$ and that of damping $\chi$,

$$n=\left\{\frac{1}{2}(\varepsilon+\sqrt{\varepsilon^2+(4\pi\sigma_r/\omega)^2})\right\}^{1/2},$$
$$\chi=\left\{\frac{1}{2}(-\varepsilon+\sqrt{\varepsilon^2+(4\pi\sigma_r/\omega)^2})\right\}^{1/2}, \quad (5)$$
$$\varepsilon=n^2-\chi^2,\ 2n\chi=4\pi\sigma_r/\omega,\ k=\frac{\omega}{c}(n-i\chi).$$

The depth of penetration of the wave into a plasma, which is well known as "skin depth", $\delta$, is given as follows.

$$\delta=1/\mu=c/2\omega\chi, \quad (6)$$

where $\mu$ is the damping coefficient.

From these equations both the electrical conductivity and the skin depth were calculated, using the measured electron temperature and its density. In the estimation of the effective collision frequency, we have used the collision cross section, $\sigma_{el}=1.0\times10^{-15}$ cm$^2$ from ref. 17), because the elastic collision with nitrogen molecules is most dominant in the temperature T=6000~7000°K. In **Fig. 28** $\sigma_r$, $\sigma_i$ and $\delta$ are plotted for various transmitted powers. $\delta$ is about 1~2 mm and comparable with the plasma radius, $r_0$=D/2 (**Fig. 17**). From eq. (4) $\sigma_r/\sigma_i=\nu_{eff}/\omega\simeq4$. In an RF plasmotron, it is generally so large, $\sigma_r/\sigma_i\gg1$ and for an optical plasmotron it becomes $\sigma_r/\sigma_i\ll1$. At the same time $\delta\gg r_0$ holds for the former device and $\delta\gg r_0$ for the latter. Most of the theoretical investigations on HF discharges in an atmospheric

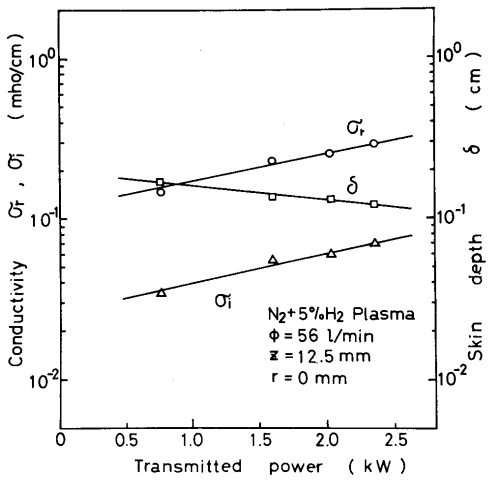


Fig. 28. Plasma conductivity calculated from the data in Fig. 26 for various transmitted powers. $\sigma_r$ is the real part of the conductivity and $\sigma_i$ is its imaginary part. Skin depth $\delta$ of the wave is also plotted in the figure.

pressure are devoted in these extreme cases and they can surely be adopted quite precisely to the RF plasmotron or optical one.

For the intermediate case, Yu. P. Raizer gives an analysis on the propagation of the discharge wave in a steady state regime[18]. His analysis is based on the experimental results of Beust and Ford[19] who have observed the moving of the arc formed in a rectangular wave guide system.

Following this model, we will calculate the energy flux, $S_1$ of the microwave, which is necessary to heat a plasma to the temperature T and them compare the result with the experimental one.

Suppose that the electromagnetic wave propagtes along the z-axis through cold gas having initial density, $\rho_0$ and velocity, u in the wave direction, and it penetrates a little into the plasma region. It is also assumed that the radial extent of the wave, $r_0$, is same as that of the plasma region (see **Fig. 29**). Then the steady state thermodynamic process occurring in this system is described by the energy balance equation:

$$\rho_0 u c_p \frac{\partial T}{\partial z} = \frac{\partial}{\partial z}\left(\kappa \frac{\partial T}{\partial z}\right) + \frac{1}{r} \times \frac{\partial}{\partial r}\left(r\kappa \frac{\partial T}{\partial r}\right) + Q, \tag{7}$$

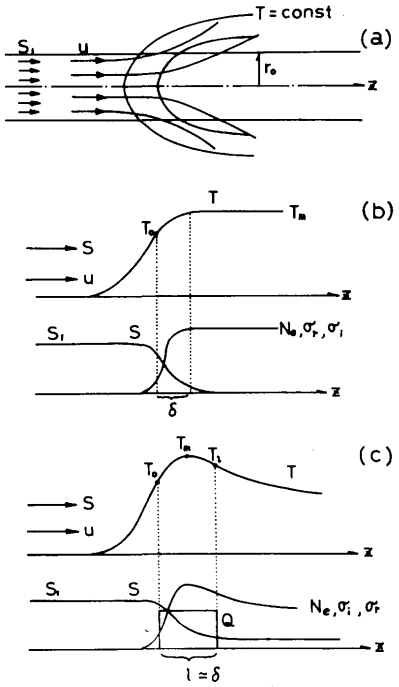


Fig. 29. Schematic representation of energy transfer processes at the boundary of a plasma. (a) Diagram of heat leakage and gas expansion. (b) Schematic distribution of temperature T (upper curve) and electron density Ne, conductivity $\sigma_r$, $\sigma_i$ and radiation flux S (lower curves) in case of no loss in the radial direction ($\delta \ll r_0$). (c) Schematic distribution of T, S and heat release Q in the presence of energy losses in the radial direction ($\delta \simeq r_0$).

$$Q = \mu S = -\frac{dS}{dz}. \tag{8}$$

Here $c_p$ = specific heat; $\kappa$ = thermal conductivity; $S = \frac{1}{4\pi}\overline{EH}$ = energy flux of the wave averaged over the period of the field. We have neglected energy loss of radiation, because the plasma temperature is relatively low. Moreover we have considered the plasma front is flat and the radial component of the gas velocity is much smaller than the axial one. Then $v_r = 0$, $\rho v_z = \rho_0 u = \text{const}$.

To avoid the complexity of the problem due to the two-dimensionality of the process, a simplified one-dimensional problem is considered by averaging eq. (7) over the cross section of the plasma channel. The second term of the right-hand side of eq. (7) can be represented in the following form[20]

$$\left(\frac{2}{r_0}\right)\left(\kappa \frac{\partial T}{\partial r}\right)_{r=r_0} = -A\Theta/r_0^2, \tag{9}$$

where $\Theta = \int_0^T \kappa dT$ = heat flux potential corresponding to the mean temperature, T of the channel at the point z and A = numerical coefficient determined by the radial profile of the temperature. The maximum value of A, $A_{max} = 5.8$, corresponds to the case $T(r_0) = 0$. When the skin depth $\delta$ of the field is much smaller than the width of the plasma region $r_0$, $\delta \ll r_0$, the thermal conduction losses in the radial direction can be neglected and we may put A = 0. **Fig. 29 (b)** shows a schematic distribution of T, $N_e$ and S etc. in the case of no loss ($A = 0$ or $\delta \ll r_0$). In the case $\delta \simeq r_0$, they will have a distribution as sketched in **Fig. 29 (c)**, since the effect of the conduction loss in the radial direction becomes appreciable ($A \neq 0$), and a similar profile of the temperature distibution is obtained in our experiment (**Fig. 24**).

Eq. (7) is rewritten in the following form

$$\frac{\rho_0 u c_p}{\kappa}\frac{d\Theta}{dz} = \frac{d^2\Theta}{dz^2} + Q - \frac{A\Theta}{r_0^2} \tag{10}$$

The analytic solution of eq. (10) is obtained in ref. 18) with the following boundary conditions,

$$Q = 0 \text{ for } T < T_0,\ z < 0 \text{ or } T < T_1,\ z > l \tag{11}$$

$$Q = \text{const. for } 0 \leqq z \leqq l,$$

where $T_0$ = the plasma forming temperature and Q is physically rewritten as follows,

$$Q = \alpha S_1 / l, \quad l = \gamma\delta, \tag{12}$$

with $\alpha$ and $\gamma$ of the order of unity. In ref. 18) calculation of the energy flux to elevate the plasma temperature to $T_m$ are performed under the assumption, $a=(\Theta(T_m)/(\Theta(T_o))-1 \ll 1$, and it is applied to the heated air from the results of Beust and Ford. Making a substitution of our experimental data of $\delta$ and $r_0$ for various temperatures combined with the transmitted power (**Fig. 26**), the theoretical curves are obtained as shown in **Fig. 30** for various values of A. As for the estimation of $\kappa$ and $c_p$, data in refs. 21) and 22) are used, and $\alpha=1$, $\gamma=2$ are taken from the consideration in ref. 18). Naturally more energy should be introduced with the increase of A to keep the constant temperature. The experimental curve in **Fig. 30** is obtained by assuming that the wave has a uniform distribution over r=1.4 cm (see **Fig. 11,** where the half width of the radiation distribution is about 2.8 cm at z=1 cm). The agreement is not so good.

The increase of $S_1$ in the theoretical curves at the lower temperature in case of $A \fallingdotseq 0$ seems to be a curious result. This, however, comes from the fact that we have assumed the radial extent of of the wave is same with that of the plasma. In the substitution of $\delta$ or $r_0$ into eq. (10) the larger extent of the wave ($\simeq$1.4 cm) than $r_0$ which will surely bring out heating of the plasma also from the radial direction and the decrease in $S_1$ is not taken into acount. Moreover it should be noted that the plasma radius is a function of the gas flow (**Fig. 20**). With the increase of the gas flow rate it becomes smaller, while the reflected power also smaller. Then the experimental value of $S_1$ changes from 0.312 to 0.35 kW/cm$^2$ at $30 \leqq \phi \leqq 200$ *l*/min. The plasma temperature, meanwhile, is almost

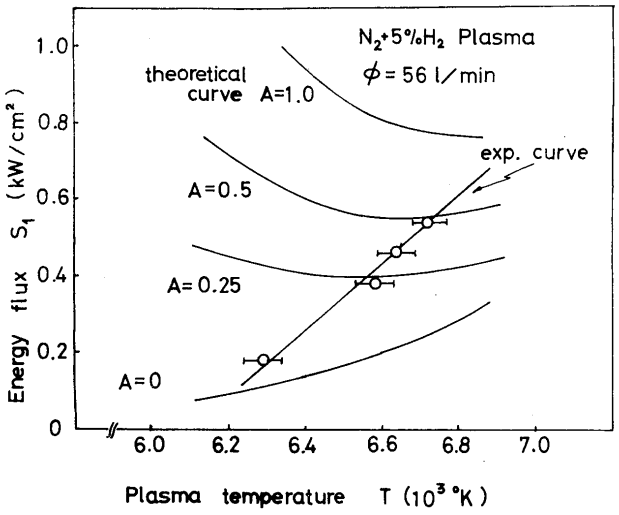


Fig. 30. Curves of incident energy flux $S_1$ necessary to heat $N_2$ plasma to a temperature T, where the plasma temperature is defined as $T_m$. Theoretical curves (A=0, 0.25, etc.) are obtained from the solution of eq. (10). Experimental curve comes from the data in Fig. 28 and it is assumed that the microwave has a uniform intensity distribution over $0 \leqq r \leqq 14$ mm (see Fig. 11).

constant in this range of the flow rate and about equal to 6650°K. Indeed the large gas flow makes it necessary to give more energy to keep a constant temperature and compensate the increase of the radial conduction loss.

From these results it seems to be more appropriate to study the heat transfer process from the absorption of the wave energy in the radial direction under the effect of a large axial gas flow, since the uniform extent of the wave is considerably large and the plasma length is in order of magnitude larger than its radius which is nearly equal to the skin depth. Of couse the axial dependence of the wave energy should be introduced in the calculation and the result will be reported elsewhere.

The result in **Figs. 15** and **16** show that the phase of the transmitted wave changes with the variation of the plasma length and a standing wave is formed at the power $P_t \simeq 0.8$ kW. This is also clarified with the standing wave meter, which shows a shift of the minimum or maximum output point towards the plasmotron in relation to that of $z_r$. Moreover $z_r=35$ mm is about equal to $\lambda_0/4$, where $\lambda_0$ is the wave length of the wave, so that the point z=0 coincides with the node of the standing wave. The current density of the plasma is described by

$$\mathbf{j}=(\sigma_r-i\sigma_i)\,\mathbf{E}_p=\mathbf{j}_r-i\mathbf{j}_i, \tag{13}$$

where $\mathbf{E}_p$ is the electric field strength in the plasma. The change of the wave phase coincides with the chage of $\mathbf{j}$, since $z_1$ in **Fig. 15** shows that the point of the maximum light emission is related with $\mathbf{j}$ and varies with $z_r$. Then the impedance of the plasma will show a similar behavior as is clearly seen in **Fig. 21.** In this figure the resistance R and the reactance X increase lineary with the transmitted power $P_t$ when $P_t \geqq 0.8$ kW. This relation must be connected with the change of the conductivity in **Fig. 28.** Experimental results show that both $\sigma_r$ and $\sigma_i$ are different for different positions in space (**Figs. 24** and **25**), while R and X give macroscopic character of the plasma over the space. So it is a difficult problem to find a proper relation between $Z=R+iX$ and $\sigma=\sigma_r-i\sigma_i$. We can only give some general interpretations on the results in **Fig. 21.**

Let's consider next three simplified cases of a coaxial line transmitting an electromagnetic wave in the principal mode; i) coaxial line with infinite center conductor, ii) coaxial line radiating into semi-infinite space and iii) change in inner radius of coaxial line. Equivalent circuits for these cases at the reference plane $T_R$ are illustrated in **Fig. 31**[23]. i) and ii) are equivalent to conductance and susceptance and iii)

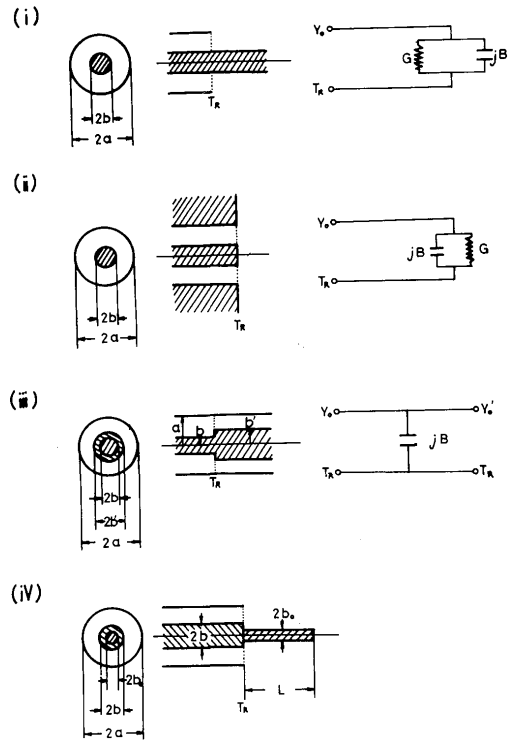


Fig. 31. Several types of coaxial waveguides. On the left the cross sectional view is sketched while in the middle the side view is written, and the equivalent circuit is shown on the wright. (i) coaxial line with infinite center conductor, ii) the line radiating into semi-infinite space, (iii) change in inner-radius of the line, (iv) model of microwave plasmtron as a coaxial line with a finite inner conductor (with a diameter $2b_0$, length L) at the open end of the line.

susceptance. For all these cases when the diameter of the inner conductor 2b is increased G and B decreases, so that the resistance, R and the capacitance, C are increased. In our plasmotron, a model of a coaxial line with a finite inner conductor of low conductivity at the reference point, $T_R$ is appropriate (**Fig. 31** iv) ). This corresponds to the case in which the above three cases are mixed. If we follow this model, the increase in the plasma diameter will bring about the increase of the plasma resistance and the reactance. The results in **Fig. 21** are in accordance with this interpretation, since the plasma diameter increases with the power $P_t$. These characteristics are also observed when the flow rate of nitrogen is varied. **Figure 22** shows R and X becomes smaller with the increase of the flow rate, while the plasma diameter also decreases as is shown in **Fig. 20.**

The plasma temperature we have obtained is 6500 ~7000°K. Similar value was already reported, using a 1.5 kW microwave plasmotron with a rectangular waveguide type[6], where the state of LTE is experimentally clarified by measuring nitrogen temperature from the absolute value or the relative intensity ratio of atomic lines and molecular band spectra of nitrogen.

Even in a large axial gas flow rate over 200 *l*/min, the plasma can exist stably with less reflection of power in our plasmotron. This is because the microwave intensity has its maximum value on the axis, where the plasma is formed. Moreover the plasma diameter changes strongly with the flow rate, though its temperature and length keep a nearly constant value. These are the remarkable features of a microwave plasmotron with a coaxial waveguide type. The plasma temperature, however, is rather low compared with a usual arc type plasma jet at the same power level. The increase of the microwave power to the plasmtron results in that of the plasma volume ($\pi D^2 L$) rather than in temperature. This is mainly because the thermal conductivity $\kappa$ of nitrogen increases sharply in the range of 5000~7000°K. This comes from the dissociation of $N_2$ into N. When the temperature is raised over 7000°K $\kappa$ decreases and the microwave power input will bring about the excess increase in temperature rather than in volume. This problem will soon be studied by using 30 kW-class plasmotron and be reported in the next paper.

## 5. Conclusion

In a 3 kW-class microwave plasmotron, a stable nitrogen plasma flame with an axial gas flow ($30 \leqq \phi \leqq 200$ *l*/min) is obtained, and its temperature is about 6700°K with its density $7 \times 10^{13}$ $cm^{-3}$, at the power level of 2.4 kW. The spatial distribution of them is rather non-uniform due naturally to the concentrated distribution of electric field in space. The higher the power input the larger the plasma volume becomes, whereas the temperature increase is moderate. The flame attains a length of about 10 cm and its diameter becomes 0.5 cm at $P_t \simeq 2.0$ kW.

A large influence of the gas flow rate on the plasma dimension and the wave transmission is observed. The increase of the flow rate causes a decrease in the diameter and also in the reflected power. The plasma temperature keeps a nearly constant value. From these results it will be considered that the decrease in .the plasma diameter results in the easier transmission of the wave with some more absorption to the plasma to keep a constant temperature.

The measured plasma impedance shows a qualitative agrrement with a model that the plasma beam acts as if it is an inner conductor with a relatively low conductivity in a coaxial waveguide.

Theoretical considerations of energy transfer processes between the wave and the plasma shows a bad coincidence with the experimental results. Much more detailed analysis is necessary to interpret precisely the experimental results. Especially it should be noted

that the large gas flow rate and the large extent of the wave give a remarkable effect on the energy balance processes.

The authors would like to thank Prof. T. Suita and Dr. M. Nishikawa for the preparation of the optical systems in our experiment.

References

1) Yu. P. Raizer, "High-Frequency High-Pressure Induction Discharge and the Electrodeless Plasmotron" Sov. Phys.—USPEKHI **12,** No. 6, 777 (1970). A review article of RF plasmotron is described in this paper.

2) H. U. Eckert and D. C. Pridmore-Brown, "Temperatme Profiles in Argon Induction Plasmas: Theory and Experiment", J. appl. Phys. **42,** No. 12, 5051 (1971).

3) J. D. Cobine and D. A. Wilbur, "The Electronic Torch and Related High Frequency Phenomena", J. appl. Phys. **22,** No. 6, 835 (1951).

4) L. Mollwo, "Electron Temperature and Electron Noise in a High-frequency Torch", Ann. Phys. (Germany) **2.,** 97 (1958).

5) S. Murayama, "Ultrahigh-Frequency Discharge in Atmospheric-Pressure Gas", J. appl. Phys. **39,** No. 12, 5478 (1968)

6) L. M. Baltin et al., "Stationary UHF-Discharge in Nitrogen at Atmospheric Pressure", Thermal phys.—High Temp. (in Russian) **9,** No. 6, 1105 (1971).

7) Yu. P. Raizer, "The Feasibility of an Optical Plasmotron and Its Power Requirments", JETP Lett. **11,** No. 3, 120 (1970).

8) N. A. Generalov et al., "Experimental Investigation of a Continuous Optical Discharge", Sov. Phys.—JETP **34,** No. 4, 763 (1972).

9) S. L. Leonard, "Evidence for Departures from Equilibrium in an RF Induction Plasma in Atmospheric-Pressure Argon", J. Quant. Spectrosc. Radiat. Transfer **12,** 619 (1972).

10) S. V. Dresvin and V. S. Klubnikin, "Investigation of Nonequilibrium in the Flow of Argon Plasma in High-Frequency Induction Discharge at Atmospheric Pressure", Thermal Phys. -High Temp. (in Russian) **9,** No. 3, 475 (1971).

11) P. L. Kapitza, "Free Plasma Filament in a High Frequency Field at High Pressure", Sov. Phys. -JETP **30,** No. 6, 973 (1970); P. L. Kapitza and S. I. Filimonov, "Apparatus for Production of a Free Plasma Filament. Determination of the Current and Resistance of the Filament", ibid. **34,** No. 3, 542 (1972).

12) Y. Arata, S. Miyake and S. Takeuchi, "Some Fundamental Characteristics of Microwave Plasma Beam as a Heat Source (1)", JWRI **1,** No. 1, 115 (1972).

13) P. L. Kapitza and L. A. Wainstein, "High-Power Electronics", p. 110 (Pergamon Press, 1966).

14) H. R. Griem, "Plasma Spectroscopy", p. 305 (Macgraw-Hill Book Co., 1964).

15) H. W. Drawin and P. Felenbok, "Data for Plasmas in Local Thermodynamic Equilibrium", p. 49 (Gauthier-Villars, 1965).

16) V. L. Ginzburg, "Propagation of Electromagnetic Waves in Plasmas" (in Russian), p. 60 (Gosudarstvenoe Izdatelstvo, 1960).

17) A. G. Engelhardt et al., "Determination of Momentum Transfer and Inelastic Collision Cross Sections for Electrons in Nitrogen Using Transport Coefficients", Phys. Rev. **135,** No. 6A, A 1566 (1964).

18) Yu. P. Raizer, "Propagation of a High-Pressure Microwave Discharge", Sov. Phys. -JETP **34,** No. 1, 114 (1972).

19) W. Beust and W. L. Ford, "Arcing in CW Transmitters", Microwave J. **10,** 91 (1961).

20) Yu. P. Raizer, "Subsonic Propazation of a Light Spark and Threshold Conditions for the Maintenance of Plasma by Radiation, "Sov. Phys.—JETP **31,** No. 6, 1148 (1970).

21) P. P. Kulik, "Coll. Essays on Physics and Chemistry of Low Temperature Plasma", L. S. Polak, Ed., (in Russian), p. 39 (Nauka, 1971).

22) K. S. Drellishak et al., "Partition Function and Thermodynamic Properties of Nitrogen and Oxygen Plasmas", Phys. of Fluids **8,** No. 9, 1590 (1965).

23) N. Marcuvitz, "Waveguide Handbook", p. 208, 213, 311 (Macgraw—Hill Book Co., 1951).